β-Arrestin2 oligomers impair the clearance of pathological tau and increase tau aggregates

Jung-A A. Woo[a,b,1], Tian Liu[a,c], Cenxiao C. Fang[a,c], Maria A. Castaño[a], Teresa Kee[a,c], Ksenia Yrigoin[a], Yan Yan[a,c], Sara Cazzaro[a,c], Jenet Matlack[a,c], Xinming Wang[a], Xingyu Zhao[a,c], David E. Kang[a,c,d,1], and Stephen B. Liggett[a,b,e,1]

[a]University of South Florida Health Byrd Alzheimer's Institute, Morsani College of Medicine, University of South Florida, Tampa, FL 33613; [b]Department of Molecular Pharmacology and Physiology, Morsani College of Medicine, University of South Florida, Tampa, FL 33613; [c]Department of Molecular Medicine, Morsani College of Medicine, University of South Florida, Tampa, FL 33613; [d]Research Division, James A. Haley Veteran's Administration Hospital, Tampa, FL 33612; and [e]Department of Medical Engineering, University of South Florida, Tampa, FL 33613

Edited by Robert J. Lefkowitz, Howard Hughes Medical Institute and Duke University Medical Center, Durham, NC, and approved January 21, 2020 (received for review October 2, 2019)

Multiple G protein-coupled receptors (GPCRs) are targets in the treatment of dementia, and the arrestins are common to their signaling. β-Arrestin2 was significantly increased in brains of patients with frontotemporal lobar degeneration (FTLD-tau), a disease second to Alzheimer's as a cause of dementia. Genetic loss and overexpression experiments using genetically encoded reporters and defined mutant constructs in vitro, and in cell lines, primary neurons, and tau P301S mice crossed with β-arrestin2$^{-/-}$ mice, show that β-arrestin2 stabilizes pathogenic tau and promotes tau aggregation. Cell and mouse models of FTLD showed this to be maladaptive, fueling a positive feedback cycle of enhanced neuronal tau via non-GPCR mechanisms. Genetic ablation of β-arrestin2 markedly ablates tau pathology and rescues synaptic plasticity defects in tau P301S transgenic mice. Atomic force microscopy and cellular studies revealed that oligomerized, but not monomeric, β-arrestin2 increases tau by inhibiting self-interaction of the autophagy cargo receptor p62/SQSTM1, impeding p62 autophagy flux. Hence, reduction of oligomerized β-arrestin2 with virus encoding β-arrestin2 mutants acting as dominant-negatives markedly reduces tau-laden neurofibrillary tangles in FTLD mice in vivo. Reducing β-arrestin2 oligomeric status represents a new strategy to alleviate tau pathology in FTLD and related tauopathies.

β-arrestin2 | tau | tauopathies | Alzheimer's disease | autophagy

Second in prevalence only to Alzheimer's disease (AD) as the cause of early onset nonvascular dementia, frontotemporal lobar degeneration (FTLD) is an aggressive neurodegenerative disease whose pathologic basis is ill defined (1). Like AD, the most common form of FTLD (FTLD-tau) displays an accumulation of hyperphosphorylated tau within inclusion bodies of neurons of the affected regions, including the cortex and temporal lobes and some subcortical neurons (2). In contrast to AD, where amyloid β (Aβ) is an integral part of the tangle, there is no accumulation of Aβ in FTLD neurons, but rather in most forms, a marked accumulation of tau is observed. Interestingly, even in AD, tau appears to be indispensable for Aβ to transduce neurotoxic signals (3, 4). Indeed, tauopathy correlates significantly better than Aβ with cognitive deficits in AD (5–7). This pathogenic role for tau in AD, and several reported observations regarding G protein-coupled receptors (GPCRs) in the pathology and treatment of AD, has prompted us to consider how GPCRs and associated proteins integrate into the tauopathy of FTLD, where unique therapeutic strategies are lacking to date.

GPCRs initiate a wide range of physiological processes, and several GPCRs have been shown to potentially play roles in AD pathogenesis (8–15). Genetic and pharmacological studies indicate that neuronal expression and/or activation of several GPCRs with diverse structures, endogenous agonists, and cell signaling effects positively contribute to Aβ and/or tau pathogenesis in animal models (8–15). However, it is not clear how this heterologous array of GPCRs can impinge on Aβ and tau pathogenesis and neurodegeneration in AD. One potential commonality among these receptors is their interaction with arrestins. Upon agonist binding (16), most GPCRs become phosphorylated by G protein-coupled receptor kinases, and the phosphorylated receptors are substrates for the binding of arrestins. These proteins physically interdict between receptor and G protein, partially uncoupling the activated receptor from its functional transducer. This phenomenon is thought to be a mechanism to regulate function within the complex signaling environment of the cell. Agonist activation also induces receptor internalization and promotes additional signals, which have been shown to be due to arrestins acting as multifunctional adapter and scaffolding proteins. Arrestins constitute a small family of four homologous proteins, known as Arrestin1, Arrestin2 (β-arrestin1), Arrestin3 (β-arrestin2), and Arrestin4 (16–18). While Arrestin1 and Arrestin4 bind to only a few receptors (rhodopsin and the color opsins) and are expressed in specific cell types (19, 20), β-arrestin1 and β-arrestin2 are ubiquitously expressed and show the highest levels of expression in the brain and spleen. β-Arrestins exist in three distinct states in cells: 1) free unbound, 2) GPCR bound, and 3) microtubule bound, each with the potential for different signaling capabilities (21–26). Previous studies have shown that β-arrestin2 is increased in AD brains (27). In addition, genetic studies have demonstrated that endogenous β-arrestin2 promotes Aβ production and deposition by physically interacting

Significance

Frontotemporal lobar degeneration (FTLD) is second only to Alzheimer's disease as a cause of dementia, and we find the scaffolding protein β-arrestin2 is elevated in human brains with this condition, and is responsible for accumulation of pathological tau tangles. Increased β-arrestin2 impairs tau clearance and promotes tau aggregation by impeding the autophagy cargo carrier p62/SQSTM1. Such activity requires β-arrestin2 in its oligomeric form, an assembly state that is not involved with receptor binding. Virus delivered gene therapy to the brain with dominant-negative mutant β-arrestin2s ablates pathologic tau in neurons of a mouse model of FTLD-tau, revealing a strategy to mitigate tauopathy by targeting β-arrestin2 oligomerization.

Author contributions: J.-A.A.W., D.E.K., and S.B.L. designed research; J.-A.A.W., T.L., C.C.F., M.A.C., T.K., K.Y., Y.Y., S.C., J.M., X.W., and X.Z. performed research; J.-A.A.W., T.L., C.C.F., M.A.C., T.K., K.Y., Y.Y., S.C., J.M., D.E.K., and S.B.L. contributed new reagents/analytic tools; J.-A.A.W., T.L., C.C.F., M.A.C., T.K., K.Y., Y.Y., S.C., J.M., X.W., X.Z., D.E.K., and S.B.L. analyzed data; and J.-A.A.W., D.E.K., and S.B.L. wrote the paper.

The authors declare no competing interest.

This article is a PNAS Direct Submission.

[1]To whom correspondence may be addressed. Email: jungaw@usf.edu, dkang@usf.edu, sliggett@usf.edu.

This article contains supporting information online at https://www.pnas.org/lookup/suppl/doi:10.1073/pnas.1917194117/-/DCSupplemental.

with the Aph-1 subunit of the γ-secretase complex (27) linking β-arrestin2 to Aβ pathogenesis (27). Prior to the current work, however, it was not known whether, or how, β-arrestin2 pathogenically impinges on tauopathy and neurodegeneration in AD, or in FTLD where there is no accumulation of Aβ.

Results

Increased β-Arrestin2 Levels in Brains of FTLD-Tau Patients and Tau P301S Transgenic Mice. We compared the expression of β-arrestin2 from the frontal cortex of aged-matched control subjects (n = 12) and patients with FTLD and tauopathy (FTLD-tau, n = 10). Western blotting for RIPA soluble β-arrestin2 demonstrated an ∼1.8-fold increase in β-arrestin2 protein in the frontal cortex of FTLD-tau patients compared to healthy controls (Fig. 1 *A* and *B*). Likewise, qRT-PCR showed a similar increase in β-arrestin2 mRNA in FTLD-tau brain samples compared to the non-FTLD-tau controls (Fig. 1*C*). We also confirmed that RIPA insoluble β-arrestin2 protein levels positively correlate with tau levels in FTLD-tau brains (Fig. 1*D* and *SI Appendix*, Fig. S1). Next, we assessed the expression of β-arrestin2 in the tau P301S transgenic mouse. This mouse overexpresses the disease-associated P301S tau in neurons and displays FTLD-like pathophysiology and behavior without Aβ accumulation (28). β-Arrestin2 protein and mRNA were significantly elevated in tau P301S transgenic mouse brains compared to non-transgenic littermates (Fig. 1 *E*–*G*). To confirm these results in a different way, cultured days in vitro (DIV)21 primary hippocampal neurons derived from tau P301S and wild-type (WT) littermates were stained for β-arrestin2 (Fig. 1*H*). Quantification of β-arrestin2 confirmed in the cell type of interest what was observed in the homogeneous brain tissue (Fig. 1*I*).

β-Arrestin2 Increases Tau Stability. We next determined whether the observed increase in β-arrestin2 in these tauopathy models can act to regulate tau in a negative (compensatory) or positive (disease enhancing) manner. In HeLa cells stably expressing tau (V5-tagged 4R0N tau, termed HeLa-V5-tau cells), transfected β-arrestin2 significantly increased total tau and phosphorylated tau (Fig. 2 *A*–*D*), and β-arrestin2 siRNA transfection significantly reduced total tau and phospho-tau (Fig. 2 *E* and *F*). Similarly, infection of tau P301S cortical primary neurons with β-arrestin2 packaged adenovirus also increased total tau and phospho-tau intensities compared to the control adenovirus condition as assessed by immunocytochemical imaging (Fig. 2 *G*–*I*) and immunoblotting (*SI Appendix*, Fig. S2 *A* and *B*). Conversely, lentivirus-mediated shRNA knockdown of β-arrestin2 reduced total tau as assessed by imaging (Fig. 2 *J* and *K*) and immunoblotting (*SI Appendix*, Fig. S2 *C* and *D*). No significant differences in tau mRNA levels were seen by β-arrestin2 overexpression or knockdown (*SI Appendix*, Fig. S2 *E* and *F*). The aforementioned studies were conducted in the absence of any GPCR agonists, which focused our attention on nonreceptor mechanisms by which β-arrestin2 interacts with tau or other partners to evoke the phenotype. We then examined tau turnover as a potential mechanism by which increased β-arrestin2 increases the effective levels of tau at steady state. Treatment of HeLa-V5-tau cells with cycloheximide to block protein translation showed that transfected β-arrestin2 significantly delays the turnover of tau (Fig. 2 *L* and *M*), consistent with β-arrestin2 stabilizing tau via scaffolding protein:protein interactions.

Genetic Reduction of *β-Arrestin2* Mitigates Tauopathy and Synaptic Dysfunction in Tau P301S Mice. The above data suggested that increased tau increases β-arrestin2, which in turn acts to further potentiate tau-mediated events by stabilizing the protein, thus indicative of a vicious positive pathogenic feedback cycle. This suggested a therapeutic attack point, should mice display the expected pathologic phenotypes when β-arrestin2 is genetically reduced. Thus, to assess the physiological relevance of endogenous β-arrestin2 in tau regulation in vivo, we crossed the tau P301S transgenic mice to *β-arrestin2*$^{-/-}$ (*Arrb2*$^{-/-}$) mice. We first fractionated (29) 7-mo-old tau P301S, tau P301S/*Arrb2*$^{+/-}$, and tau P301S/*Arrb2*$^{-/-}$ littermate mouse brains. Sarkosyl-insoluble tau was clearly decreased in tau P301S/*Arrb2*$^{+/-}$ and tau P301S/*Arrb2*$^{-/-}$ compared to tau P301S littermates. However, there was no difference in the sarkosyl-soluble tau (Fig. 3 *A*–*C*). Immunohistochemistry for

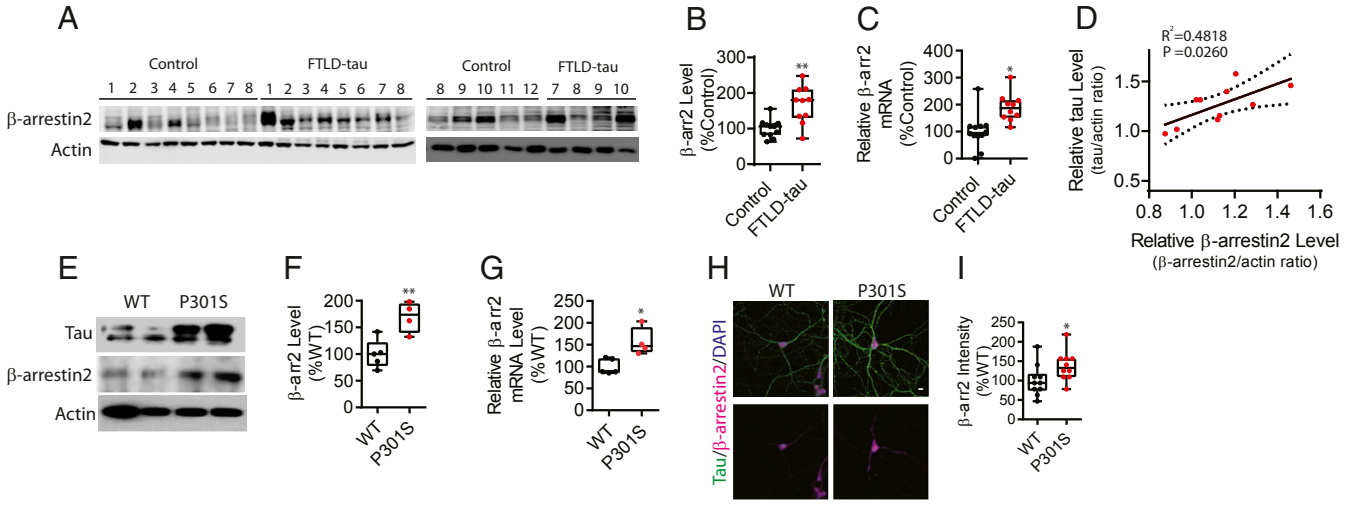

Fig. 1. β-Arrestin2 is increased in brains of FTLD-tau patients and tau P301S transgenic mice. (*A*) Representative immunoblots of β-arrestin2 from the frontal cortex of 12 age-matched unaffected controls and 10 FTLD-tau patients. The numbers above the lanes are sample numbers corresponding to the subjects, with some samples repeated on the second gel. (*B* and *C*) Quantification of β-arrestin2 protein and mRNA levels in the frontal cortex of FTLD-tau patients compared with unaffected controls (n = 12 healthy control, n = 10 FTLD-tau, $^{**}P < 0.005$, $^{*}P < 0.05$). (*D*) Correlation of insoluble tau and β-arrestin2 expression in FTLD-tau patients (n = 10 FTLD-tau). Each data point represents mean results from duplicate determinations from a given subject. The blots are shown in *SI Appendix*, Fig. S1. (*E*) Representative immunoblots of β-arrestin2 in the mouse cortex from 7-mo-old WT and tau P301S transgenic littermates. (*F* and *G*) Quantification of β-arrestin2 protein and mRNA levels in the cortex of WT and tau P301S transgenic littermates (n = 5 WT, n = 4 tau P301S, $^{**}P < 0.005$, $^{*}P < 0.05$). (*H*) Representative staining of β-arrestin2 (magenta) and total tau (green) using DIV21 hippocampal primary neurons derived from WT and tau P301S littermates. (Scale bar: 10 μm.) (*I*) Quantification of β-arrestin2 immunoreactivity (n = 3 independent experiments, $^{*}P < 0.05$).

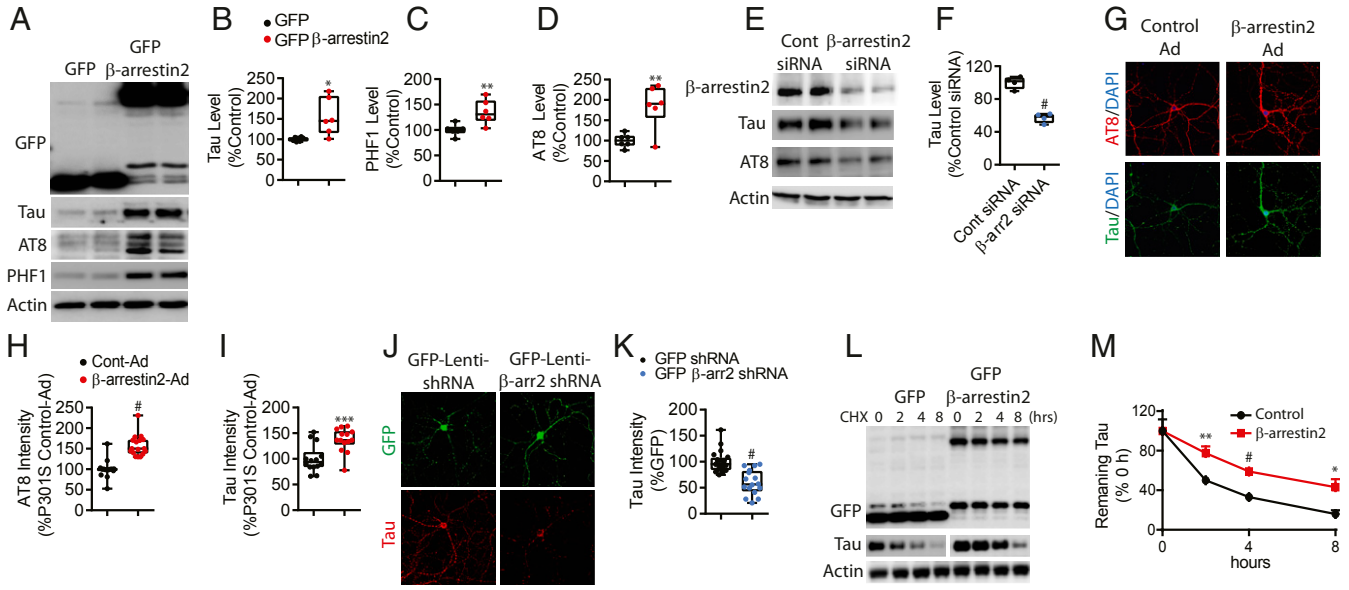

Fig. 2. Overexpression and knockdown of β-arrestin2 modulates tau levels. (*A*) Representative immunoblots of the indicated proteins in HeLa-V5-tau cells transiently transfected with GFP or GFP-β-arrestin2. (*B–D*) Quantification of tau, PHF1, and AT8 levels from six experiments (*$P < 0.05$, **$P < 0.005$ vs. GFP). (*E*) Representative immunoblots of the indicated proteins in HeLa-V5-tau cells transiently transfected with either control siRNA or β-arrestin2 siRNA. (*F*) Quantification of tau levels from four experiments ($^{\#}P < 0.0001$). (*G*) Representative staining of tau (green) and AT8 (red) in hippocampal primary neurons from tau P301S transgenic mice transduced with either control or β-arrestin2 adenovirus. (Scale bar: 10 μm.) (*H* and *I*) Quantification of AT8 and total tau immunoreactivities from three independent experiments, $^{\#}P < 0.0001$, ***$P < 0.0005$). (*J*) Representative staining of tau (red) in hippocampal primary neurons from tau P301S transgenic mice transduced with either GFP-lenti shRNA or GFP-lenti β-arrestin2 shRNA. (*K*) Quantification of total tau immunoreactivity ($n = 4$ independent experiments, $^{\#}P < 0.0001$). (*L*) Representative immunoblots of indicated proteins from HeLa-V5-tau cells transfected with GFP or GFP-β-arrestin2 and treated with cycloheximide (100 μg/mL) for indicated times. (*M*) Quantification of tau levels with cycloheximide treatment ($n = 4$; **$P < 0.005$, $^{\#}P < 0.0005$, *$P < 0.05$, repeated measures ANOVA, followed by Bonferroni post hoc tests).

phospho-tau (pS199/pS202) was performed with cortex (Fig. 3 *D* and *E*) and hippocampus (Fig. 3 *D* and *F*) of 7-mo-old WT, tau P301S, tau P301S/*Arrb2*$^{+/-}$, and tau P301S/*Arrb2*$^{-/-}$ littermates. We found that brain sections from tau P301S/*Arrb2*$^{+/-}$ and tau P301S/*Arrb2*$^{-/-}$ mice exhibited ~50% less phospho-tau immunoreactivity compared to those from tau P301S mice (Fig. 3 *D–F*). We also confirmed that knockout of *β-arrestin2* decreases sarkosyl-insoluble tau in cultured primary neurons derived from brains of the tau P301S/*Arrb2*$^{-/-}$ mice compared to those from tau P301S mice (*SI Appendix*, Fig. S3 *A–C*).

To determine functional changes in synaptic plasticity imposed by the genetic decrease in expressed β-arrestin2, we carried out electrophysiological studies on brain slices. Input-output (IO) analysis indicated no significant differences among WT, tau P301S, tau P301S/*Arrb2*$^{+/-}$, and tau P301S/*Arrb2*$^{-/-}$ littermate slices (Fig. 3*G*), as expected from previous electrophysiological studies of tau P301S mice (28–30). In paired pulse facilitation (PPF) studies, we observed significant field excitatory postsynaptic potential (fEPSP) slope reductions in tau P301S slices in all interstimulus intervals (except 260 to 280 ms) compared to WT slices (Fig. 3*H*), with tau P301S/*Arrb2*$^{+/-}$ as well as tau P301S/*Arrb2*$^{-/-}$ slices being not appreciably different from tau P301S slices (Fig. 3*H*). In contrast, in long-term potentiation (LTP) recordings using theta burst stimulation, tau P301S slices were markedly impaired in the induction and maintenance of LTP compared to WT slices as expected (29). However, LTP in tau P301S/*Arrb2*$^{+/-}$ and tau P301S/*Arrb2*$^{-/-}$ slices was restored to levels virtually identical to those of WT slices (Fig. 3*I*). These results suggest that the cycle can be broken at the β-arrestin2 interface. As further evidence for a salutary effect of lowering β-arrestin2 and consistent with the LTP data, silencing of *β-arrestin2* by shRNA lentivirus significantly rescued the depletion of synaptophysin (presynaptic; *SI Appendix*, Fig. S3 *D* and *E*) and drebrin (postsynaptic; *SI Appendix*, Fig. S3 *D* and *F*) compared to tau P301S primary neurons transduced with control shRNA lentivirus.

β-Arrestin2 Oligomerization Is Required for Tau Stability. It has been shown that β-arrestin2 can be found as an oligomer in multiple cell types (31, 32). Inositol hexakisphosphate (IP6) enhances this self-association of β-arrestin2 by bridging neighboring molecules in a head-to-tail configuration. Positively charged arginine and lysine residues within the N terminus and C terminus of β-arrestin2 were found to be critical for both IP6 binding and oligomerization. Given the physical overlap of IP6 and GPCR binding sites, β-arrestin2 binding to an activated GPCR and to IP6 is mutually exclusive, indicating that in the oligomeric form β-arrestin2 may serve other purposes apart from GPCR binding (33–43).

We tested the hypothesis that β-arrestin2 self-oligomerization affects tau stability and tauopathy by using a β-arrestin2 N-terminal domain mutant (K158A, K161A, and R162A, referred to as β-arrestin2 ΔIP6N), and a C-terminal domain mutant (K232A, R234A, K252A, K326A, and K328A, referred to as β-arrestin2 ΔIP6C); these mutants are incapable of forming oligomers as determined by BRET and coimmunoprecipitation assays (31, 32), but nevertheless bind to activated GPCRs with WT affinity (44).

When DIV18 tau P301S cortical primary neurons were transduced with either β-arrestin2 ΔIP6C or ΔIP6N lentivirus, a ~50% reduction in tau compared to control was evident (Fig. 4 *A* and *B*), which represents a key finding relevant to both mechanism of action and potential therapeutic strategies. Consistent with these findings, YFP-β-arrestin2 ΔIP6C and YFP-β-arrestin2 ΔIP6N expression in HeLa-V5-tau cells also caused significant reductions in tau as assessed by immunocytochemistry (*SI Appendix*, Fig. S4*A*). To show that these mutants act as dominant negatives for oligomerization, we performed proximity ligation assays (PLAs) examining the interaction between β-arrestin2-flag

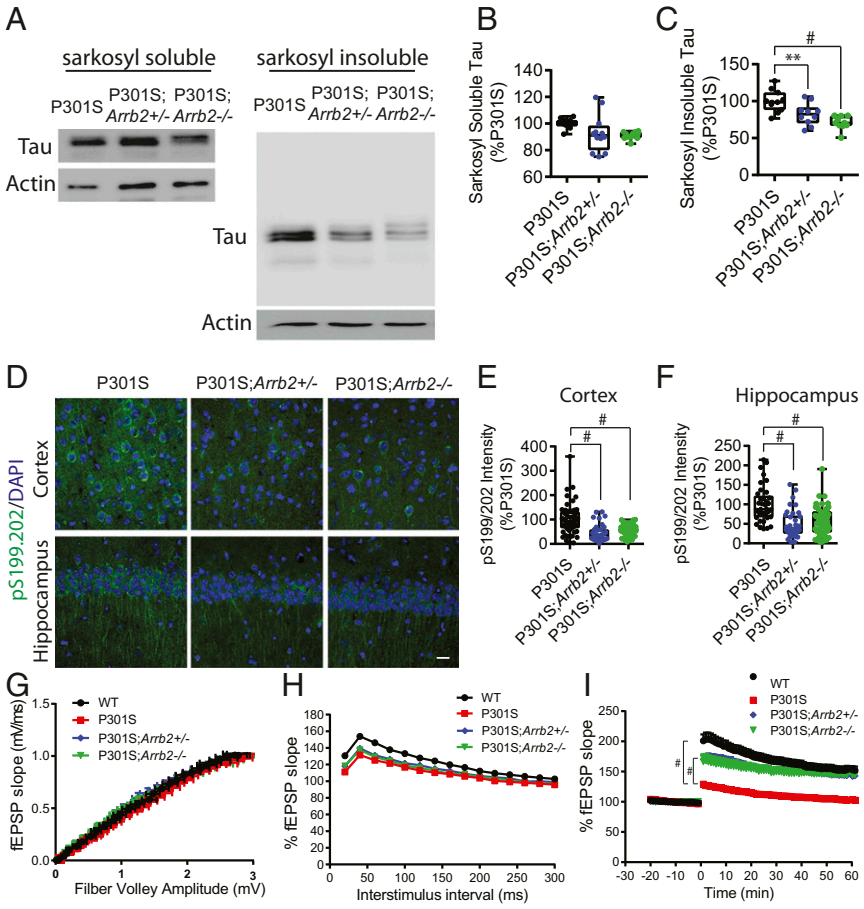

Fig. 3. Genetic reduction in β-arrestin2 mitigates neuronal tauopathy. (*A*) Representative immunoblots for sarkosyl-soluble and sarkosyl-insoluble tau from brains of 7-mo-old tau P301S, tau P301S/*Arrb2*$^{+/-}$, and tau P301S/*Arrb2*$^{-/-}$ littermates. (*B* and *C*) Quantification of four experiments performed as shown in *A*, $^{**}P < 0.005$, $^{\#}P < 0.0001$. (*D*) Representative staining of phospho-tau, pS199/202 (green) in hippocampus, and cortex of 7-mo-old tau P301S, tau P301S/*Arrb2*$^{+/-}$, and tau P301S/*Arrb2*$^{-/-}$ mice. (Scale bar: 20 μm.) (*E* and *F*) Quantification of pS199/202 immunoreactivity in cortex and hippocampus ($n = 4$/genotype, $^{\#}P < 0.0001$). (*G*) IO analysis generated by stepping up stimulation amplitude from 1 to 15 mV in WT, tau P301S, tau P301S/*Arrb2*$^{+/-}$, and tau P301S/*Arrb2*$^{-/-}$ acute slices ($n = 35$ to 46 slices/genotype from four mice/genotype). (*H*) PPF showing fEPSP slope as a function of 30- to 300-ms interstimulus interval ($n = 38$ to 49 slices/genotype from four mice/genotype). (*I*) LTP induced by theta burst stimulation showing significant differences in fEPSP slope between tau P301S compared to WT, tau P301S/*Arrb2*$^{+/-}$, and tau P301S/*Arrb2*$^{-/-}$ slices ($n = 25$ to 43 slices/genotype from four mice/genotype, $^{\#}P < 0.0001$).

and β-arrestin2-myc in presence of control vector, or β-arrestin2 ΔIP6C or β-arrestin2 ΔIP6N. Indeed, β-arrestin2 ΔIP6C and β-arrestin2 ΔIP6N significantly reduced β-arrestin2-flag and β-arrestin2-myc interaction (*SI Appendix*, Fig. S4 *B* and *C*). These results confirmed the oligomerization of WT β-arrestin2 in the control setting and showed displacement of WT β-arrestin2 from the oligomer by expression of either the ΔIP6C or the ΔIP6N mutants (*SI Appendix*, Fig. S4 *B* and *C*). We further investigated whether β-arrestin2 oligomerization is required for slowing tau turnover by disrupting oligomerization using these mutants in

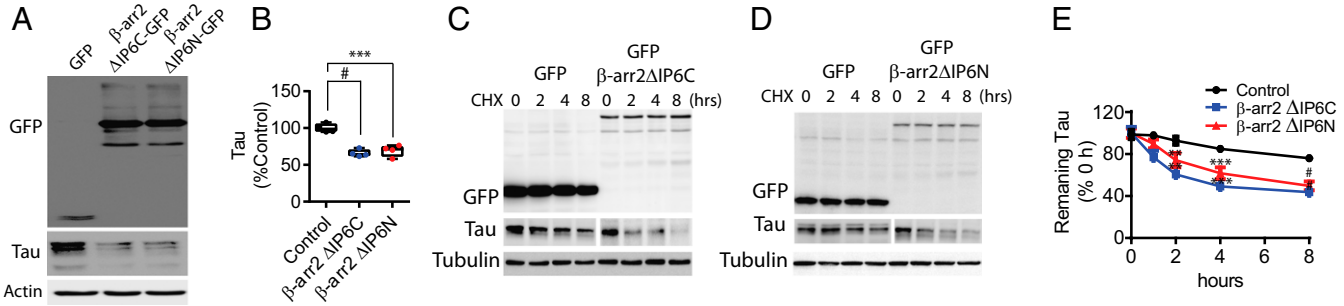

Fig. 4. β-Arrestin2 oligomerization is required for suppressing tau turnover. (*A*) Representative immunoblots of DIV18 cortical primary neurons from tau P301S transduced with GFP, β-arrestin2 ΔIP6C-GFP, or β-arrestin2 ΔIP6N-GFP at DIV5. (*B*) Quantification of tau level ($n = 4$, $^{\#}P < 0.0001$, $^{***}P < 0.0005$). (*C* and *D*) Representative immunoblots of indicated proteins in HeLa-V5-tau cells transfected with control vector, β-arrestin2 ΔIP6C,and β-arrestin2 ΔIP6N treated with cycloheximide (100 μg/mL) for indicated times. (*E*) Quantification of tau levels with cycloheximide treatment ($n = 4$; $^{**}P < 0.005$, $^{***}P < 0.0005$, $^{\#}P < 0.0001$, repeated measures ANOVA, followed by Bonferroni post hoc).

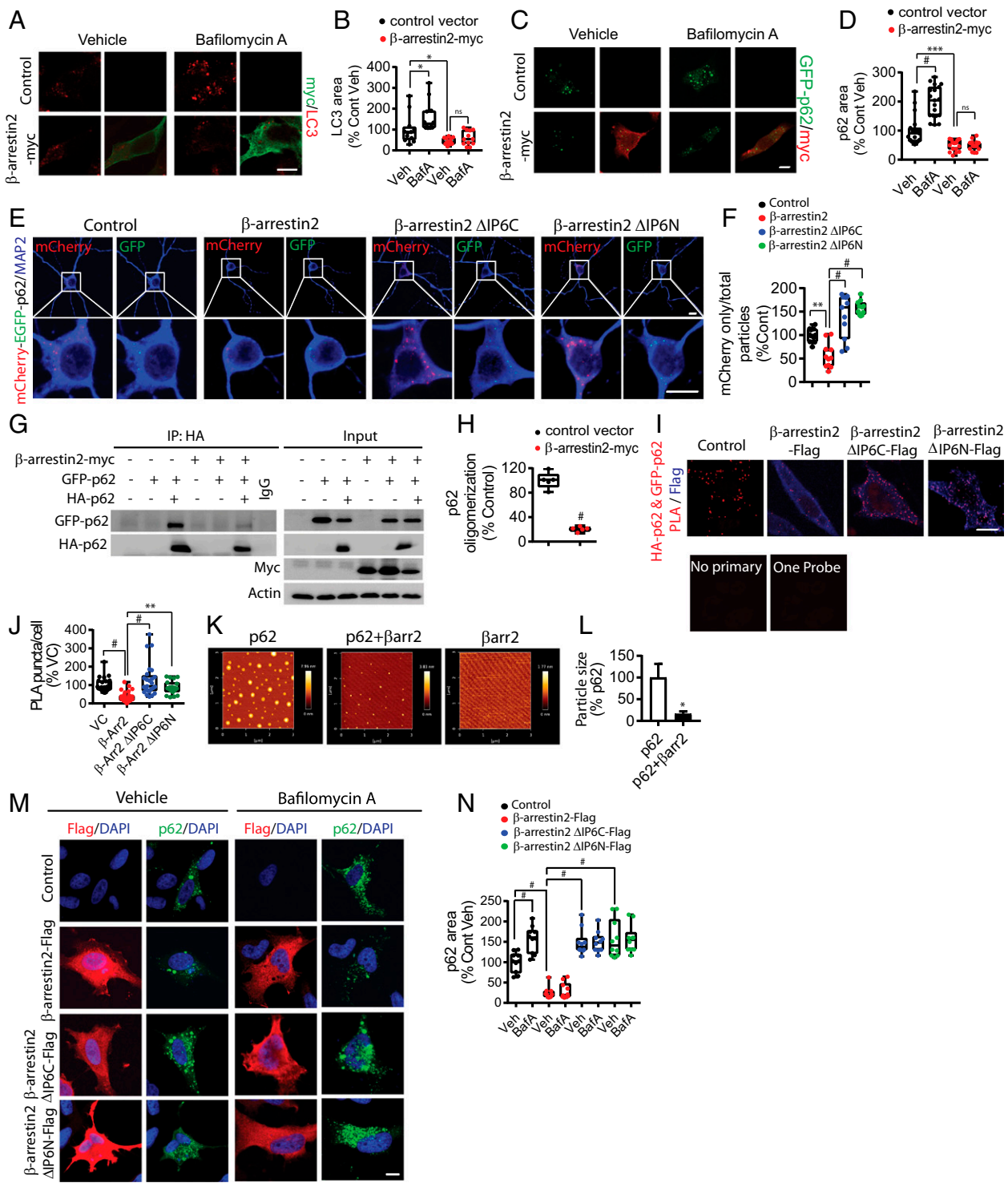

Fig. 5. β-Arrestin2 oligomerization inhibits p62-mediated tau degradation. (*A*) Representative images of LC3-positive autophagosomes from HeLa-V5-tau cells transiently transfected with control vector or β-arrestin2-myc with/without 100 nM of bafilomycin A1. (Scale bar: 10 μm.) (*B*) Quantification of LC3 puncta ($n = 4$ independent experiments, $^{*}P < 0.05$). (*C*) Representative images of GFP-p62 positive autophagosomes from HeLa-V5-tau cells transiently transfected with control vector or β-arrestin2-myc with/without 100 nM of bafilomycin A1. (Scale bar: 10 μm.) (*D*) Quantification of GFP-p62 puncta ($n = 4$ independent experiments, $^{\#}P < 0.0001$, $^{***}P < 0.0005$). (*E*) Representative images of DIV21 tau P301S hippocampal primary neurons transduced with mcherry-GFP-p62 AAV9 with control, β-arrestin2, β-arrestin2 ΔIP6C, or β-arrestin2 ΔIP6N lentivirus at DIV5. (*F*) Quantification of mCherry-only particles ($n = 3$ independent experiments, $^{**}P < 0.005$, $^{\#}P < 0.0001$). (*G*) Representative immunoblots of HeLa-V5-tau cells transiently transfected with control vector or β-arrestin2-myc with either GFP-p62 and/or HA-p62 and subjected to lysis followed by co-IP. (*H*) Quantification of GFP-p62 and HA-p62 interaction by co-IP ($n = 5$ independent experiments, $^{\#}P < 0.0001$). (*I*) Representative images of PLA of HeLa-V5-tau cells transfected with control vector, β-arrestin2, β-arrestin2 ΔIP6C, or β-arrestin2 ΔIP6N. (Scale bar: 10 μm.) (*J*) Quantification of PLA puncta ($n = 4$ independent experiments, $^{\#}P < 0.0001$, $^{**}P < 0.005$). (*K*) A total of 0.4 μg of p62 was incubated with/without 0.2 μg of β-arrestin2 for 2 h at room temperature prior to AFM imaging. (*L*) Quantification of p62 particle size ($n = 3$ independent experiments, $^{*}P < 0.05$). (*M*) Representative staining of flag (red) in HeLa-V5-tau cells transfected with control vector, β-arrestin2-flag, β-arrestin2 ΔIP6C-flag, or β-arrestin2 ΔIP6N-flag with GFP-p62 with/without 100 nM of bafilomycin A treatment. (Scale bar: 10 μm.) (*N*) Quantification of GFP-p62 puncta ($n = 4$ independent experiments, $^{\#}P < 0.0001$).

several models. Studies with the β-arrestin2 ΔIP6C and β-arrestin2 ΔIP6N mutants showed enhancement of tau turnover in the cycloheximide chase experiments (Fig. 4 *C*–*E*). To determine whether β-arrestin2 oligomerization status alters tau aggregation itself, we performed filter-trap assays from HeLa-V5-tau cells transfected with β-arrestin2 variants, in which tau aggregates from detergent-soluble and -insoluble lysates were captured by cellulose acetate membranes and assessed by immunoblotting. While detergent-soluble lysates showed little to no aggregates, detergent-insoluble lysates derived from β-arrestin2 ΔIP6C or ΔIP6N transfected cells showed significantly reduced tau aggregates compared to control vector transfected cells (*SI Appendix*, Fig. S4 *D* and *E*).

β-Arrestin2 Oligomers Interact with p62 and Inhibit p62 Self-Association. Hyperphosphorylated (and thus more "ordered") tau is thought to undergo clearance by an autophagy-lysosome pathway (45–49). To understand the mechanistic basis of β-arrestin2 in tau stabilization and accumulation, we used bafilomycin A, a lysosome inhibitor known to activate autophagy and promote the accumulation of LC3-positive autophagosomes, to test whether β-arrestin2 affects autophagy. Interestingly, overexpression of β-arrestin2 in HeLa-V5-tau cells significantly inhibited bafilomycin A-induced increase in LC3-positive puncta (Fig. 5 *A* and *B*), suggesting that β-arrestin2 inhibits autophagy at or upstream of LC3.

P62/SQSTM1 is a key autophagy cargo receptor that regulates autophagosome formation by linking its cargo (i.e., misfolded tau or Aβ) to LC3-positive autophagosomes. Indeed, p62 is associated with neurofibrillary tangles (50–53), and soluble cytoplasmic p62 levels are significantly reduced in AD brains (50, 54). Increased p62 expression improves cognitive impairments in AD animal models by enhancing autophagy induction, and genetic loss of *p62* leads to dramatic accumulation of tau and neurodegeneration (50, 54, 55). Moreover, a recent study showed that p62 expression is associated with clearance of insoluble tau (56).

P62 forms particles by self-interaction via its N-terminal PB1 domain, which is essential for its activity and is seen as puncta of different sizes in cells (57, 58). In HeLa-V5-tau cells transfected with GFP-p62, we observed an expected increase in GFP-p62 puncta upon bafilomycin A treatment (Fig. 5 *C* and *D*). However, overexpression of β-arrestin2 significantly reduced GFP-p62 puncta at both steady state and after bafilomycin, such that bafilomycin A no longer increased GFP-p62 puncta (Fig. 5 *C* and *D*). This suggested that β-arrestin2 inhibits the flux of p62 particles from their target substrates to lysosomes. To directly test this hypothesis, we utilized the mCherry-EGFP-p62 autophagy flux reporter. This reporter takes advantage of the sensitivity of GFP to low pH (which quenches the signal) and the insensitivity of mCherry to low pH. Therefore, colocalized red and green puncta are indicative of nonlysosomal p62 at steady state. However, upon fusion with lysosomes (autolysosomes), red puncta persist while green puncta dim and disappear (59, 60). In primary neurons transduced with control or β-arrestin variant lentiviruses and with high-titer rAAV9 mCherry-EGFP-p62, the ratio of mCherry only to total puncta was significantly reduced by β-arrestin2 expression (Fig. 5 *E* and *F*). Importantly, β-arrestin2 ΔIP6C and ΔIP6N mutants, acting as dominant negatives to WT β-arrestin2 oligomerization, significantly increased this measure (Fig. 5 *E* and *F*). Thus these β-arrestin2 mutants which cannot self-oligomerize (and inhibit WT-β-arrestin2 oligomerization), failed to reduce flux, confirming the notion that it is the oligomerized, non-GPCR bound, β-arrestin2 that is acting to fuel the tauopathy. Similar results of p62 autophagy flux with β-arrestin2, and β-arrestin2 ΔIP6N, were seen in HeLa-V5-Tau cells (*SI Appendix*, Fig. S5 *A* and *B*).

Given the effects on p62 autophagy flux, we tested whether β-arrestin2 physically interacts with p62. Coimmunoprecipitation (co-IP) experiments indeed showed that β-arrestin2 forms a complex with p62 (*SI Appendix*, Fig. S5*C*). Self-association of p62 via its N-terminal PB1 domain is essential for its cargo receptor activity by enabling more interaction sites (multiple binding) to its ubiquitinated cargo as well as simultaneous binding to multiple LC3 proteins (57, 58). Hence, we tested whether β-arrestin2 affects p62 self-interaction by co-IP experiments using HA-p62 and GFP-p62 constructs. β-Arrestin2 reduced p62 self-association as detected by co-IP of GFP-p62 and HA-p62 (Fig. 5 *G* and *H*). Given that β-arrestin2 oligomeric mutants, ΔIP6C and ΔIP6N, reduced tau aggregates by slowing tau turnover, we next tested whether β-arrestin2 ΔIP6C and ΔIP6N mutants affect p62 self-association by a PLA as well as co-IP. While β-arrestin2 significantly reduced the HA-p62/GFP-p62 complex PLA signal (p62 self-interaction), neither β-arrestin2 ΔIP6C nor β-arrestin2 ΔIP6N reduced HA-p62/GFP-p62 PLA puncta (Fig. 5 *I* and *J*). We also confirmed that while β-arrestin2 significantly reduced HA-p62 and GFP-p62 interaction, neither β-arrestin2 ΔIP6C nor β-arrestin2 ΔIP6N alone were capable of reducing HA-p62 and GFP-p62 interaction by co-IP (*SI Appendix*, Fig. S5*D*). In fact, both β-arrestin2 ΔIP6C and β-arrestin2 ΔIP6N show much less interaction with p62 compared to β-arrestin2 (*SI Appendix*, Fig. S5 *E* and *F*). Recent studies have shown that purified recombinant p62 spontaneously forms globular oligomers (61). To test whether β-arrestin2 can directly affect p62 oligomerization in vitro, we visualized purified recombinant p62, β-arrestin2, and p62 mixed with β-arrestin2 with atomic force microscopy (AFM). Recombinant p62 spontaneously formed visible globular particles between 5 and 100 nm in diameter (Fig. 5*K*), whereas only very few small β-arrestin2 particles were visible under identical conditions (Fig. 5*K*). When p62 was mixed together with β-arrestin2, the size of the particles was substantially reduced (Fig. 5 *K* and *L*), indicating that the inhibition of p62 self-association by β-arrestin2 reduces the size of p62 particles. Next, we tested whether β-arrestin2 oligomerization is required for bafilomycin A-induced p62 puncta formation. As expected, GFP-p62 puncta were increased upon bafilomycin A treatment in control vector transfected cells (Fig. 5 *M* and *N*). However, β-arrestin2 significantly reduced GFP-p62 puncta at both steady state and after bafilomycin A (Fig. 5 *M* and *N*). Interestingly, both β-arrestin2 ΔIP6C and β-arrestin2 ΔIP6N transfected cells showed increased GFP-p62 puncta at steady state, indicating that β-arrestin2 ΔIP6C and β-arrestin2 ΔIP6N increase the flux of p62 particles thereby increasing autophagy flux (Fig. 5 *M* and *N*).

Mutant β-Arrestin2 Viral Therapy Inhibits Tauopathy In Vivo. Given the above results, which indicate the requirement for the oligomerized forms of β-arrestin2 in tauopathy, and the dominant-negative effects of mutant β-arrestin2s that fail to oligomerize, we tested whether β-arrestin2 ΔIP6C and β-arrestin2 ΔIP6N mutants reduce tauopathy in the in vivo setting, as a potential therapeutic strategy. We generated and purified high-titer ($>1 \times 10^{12}$ vg mL^{-1}) rAAV9-expressing GFP control, GFP-β-arrestin2 ΔIP6N, and GFP-β-arrestin2 ΔIP6C. AAVs were then stereotaxically injected bilaterally into the hippocampus of 5-mo-old tau P301S mice. Two months postinjection, mouse brains were probed for detection of GFP and tau. These studies showed that GFP-β-arrestin2 ΔIP6N or GFP-β-arrestin2 ΔIP6C injection markedly reduced sarkosyl-insoluble tau compared to GFP control (Fig. 6 *A* and *C*). However, sarkosyl-soluble tau was not significantly altered by β-arrestin2 mutants (Fig. 6 *A* and *B*). Furthermore, GFP-β-arrestin2 ΔIP6N- and GFP-β-arrestin2 ΔIP6C-expressing neurons showed significant reductions in HT7-immunoreactive tau compared to GFP-expressing control or neighboring noninfected neurons (Fig. 6 *D* and *E*). Given the dominant-negative effects of these mutants (Fig. 4 *A* and *B*) (*SI Appendix*, Fig. S4 *B* and *C*), these results are consistent with their therapeutic mechanism being from effective reduction of oligomerization of the increased endogenous neuronal β-arrestin2 in the tau P301S mice. And, since the injections were given at 5 mo of age, when tau accumulation is well underway, it is apparent that this approach can reduce preexisting tau-tangle pathology.

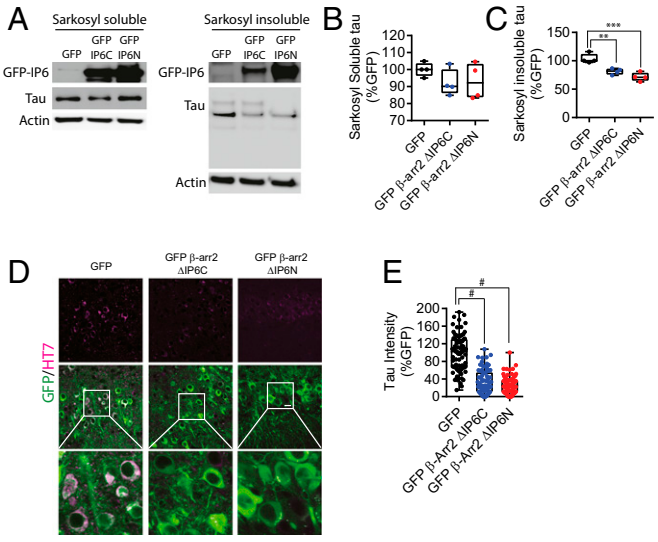

Fig. 6. Oligomerization-deficient β-arrestin2 mitigates tauopathy in vivo. (*A*) Representative immunoblots for sarkosyl-soluble and sarkosyl-insoluble tau from brains of 7-mo-old tau P301S mice stereotaxically injected with rAAV9 encoding GFP, GFP-β-arrestin2 ΔIP6C, or GFP-β-arrestin2 ΔIP6C into the hippocampus at 5 mo of age. (*B* and *C*) Quantification of sarkosyl-soluble and -insoluble tau from tau P301S mice stereotaxically injected as in *A*, $n = 4$/genotype, $^{**}P < 0.005$, $^{***}P < 0.0005$). (*D*) Representative staining of total tau (magenta) of the hippocampus of 7-mo-old tau P301S stereotaxically injected as in *A*. (Scale bar: 20 μm.) (*E*) Quantification of total tau immunoreactivities ($n = 4$/genotype, $^{\#}P < 0.0001$).

Discussion

FTLD represents a distinct clinical and pathological dementia, yet is often misdiagnosed as, or treated in a similar manner to, AD. The most obvious difference between the pathology of AD and FTLD is the absence of Aβ accumulation in FTLD. In its most common form, FTLD-tau has an accumulation of tau as a poignant feature. Given that tau levels (in AD) appear to be a better predictor of cognitive deficits (62), the tau accumulation in FTLD is presumed to also be a key factor in neurodegeneration in this disease. Agonists and antagonists to several GPCRs (M1 mAchR, adenosine receptor, β_2AR) have been proposed as potential therapy for AD (8, 63–65), and given that tau participates in both AD and FTLD, we considered ways to modulate GPCR signaling through the two β-arrestins that associate with most GPCRs. The increase in β-arrestin2 in human FTLD brains, and in the tau-overexpressing cells, indicated that this might be a fruitful approach for understanding pathogenesis and localizing a point for therapeutic interdiction. Further studies revealed several unexpected findings. First, it became apparent that β-arrestin2 can up-regulate tau, and that tau can up-regulate β-arrestin2. This suggested that the up-regulation of β-arrestin2 in human FTLD brains is maladaptive, rather than a compensatory or salutary event that might abrogate tau accumulation. Hence, this effect is a positive feedback loop, which once initiated serves to fuel further deleterious effects. In addition, it became clear that the oligomerized β-arrestin2 (which does not interact with GPCRs) was responsible for tau accumulation, which led us to examine nonreceptor functions of β-arrestin2 in the context of FTLD. Of note, β-arrestin2 has previously been shown to regulate the γ-secretase processing of APP by interacting with Aph-1, thereby positively regulating Aβ generation (27). The same studies showed that β-arrestin2 is significantly increased in AD brains and APP transgenic mice (27). In the current work, we show in cells and mice with elevated tau, β-arrestin2 is elevated. And, when β-arrestin2 is overexpressed, tau levels become elevated. Based on tau mRNA levels being unchanged, tau protein clearance was considered as a mechanism by which β-arrestin2 modulates its levels. Our data indicate that β-arrestin2 reduces tau clearance by impairing p62-mediated autophagy, a role carried out by the oligomerized form of β-arrestin2. Specifically, our results indicate that β-arrestin2 oligomers increase tau levels by blocking the self-interaction of p62, an initial step essential in p62-mediated autophagy flux. Genetic reduction or ablation of *β-arrestin2* significantly decreased sarkosyl-insoluble tau and mitigated tauopathy in vivo. Furthermore, β-arrestin2 mutants incapable of forming oligomers actually reduced insoluble tau. Such actions, which we show are due to the dominant-negative antioligomer properties of these mutants, reduced tauopathy in cultured model cells and neurons and in a FTLD-tau mouse model in vivo. These data highlight a mechanism of tau regulation by β-arrestin2 and provide a proof-of-concept strategy to mitigate tauopathy by targeting β-arrestin2 oligomerization (Fig. 7).

Boularan et al. (43) found that the β-arrestin2 ΔIP6N and ΔIP6C mutants do not form oligomers but are otherwise normal in terms of localization and binding to (and mediating internalization of) GPCRs and other partners such as AP2, Filamin A, and MAPK. To date, no previous study has implicated oligomeric β-arrestin2 in p62-mediated autophagy. Our findings indicated that β-arrestin2 reduces p62 self-interaction, number of p62 particles, and alters tau clearance. And, expression of β-arrestin2 ΔIP6N and ΔIP6C mutants increase p62 self-interaction and the number of p62 particles by impairing oligomerization of WT (endogenous) β-arrestin2. Such changes were directly related to the turnover of tau and accumulation of insoluble tau, consistent with the role of p62 in preferentially lowering insoluble tau (56). Moreover, insoluble p62 itself is associated with neurofibrillary tangles (50–53), while soluble cytoplasmic p62 levels are significantly reduced in AD brains (50, 54). Increased p62 expression improves cognitive impairments in AD animal models by enhancing autophagy induction, and genetic loss of *SQSTM1*/p62 leads to tau accumulation and neurodegeneration (50, 54, 55). P62 self-interaction represents the first step in p62 particle formation, which is essential for p62-mediated autophagy. The regulation of p62 at this step by β-arrestin2 offers an opportunity for therapeutic intervention. The observation that both IP6-binding mutants enhanced p62 self-interaction and reduced insoluble tau indicated that while β-arrestin2 oligomers block p62-mediated autophagy, β-arrestin2 monomers promote p62-mediated autophagy. If so, β-arrestin2 oligomer-to-monomer transition and vice versa may function as a regulatable molecular switch to toggle p62-mediated autophagy.

In the current experiments, the mutant β-arrestin2 proteins were highly effective at reducing tau in neurons. In individual cells of the brain where expression of ΔIP6N or ΔIP6C was verified (by their GFP tags), tau levels were essentially undetectable, which was in contrast to the remaining cells with high levels of tau. For gene therapy of human FTLD-tau, mutants with a somewhat decreased capacity for such inhibition might be desirable, so that some levels of the oligomer are present to carry out other functions. Indeed, oligomeric β-arrestin2 has been shown to facilitate nucleocytoplasmic shuttling of proteins (43). Similarly, small molecule inhibitors of β-arrestin2 oligomerization, given for treatment or prevention of FTLD-tau, could be designed to spare complete loss of the oligomer in the cell. Importantly, these strategies are not expected to alter neuronal GPCR signaling pathways, since the monomeric form of β-arrestin2 would be preserved. Based on our findings, the effects of inhibiting β-arrestin2 oligomerization would be expected to not only inhibit the development of new tau tangles, but also to clear existing tau accumulations due to this mechanism of enhancing tau clearance. Thus, this treatment strategy could be preventative for those at risk or with mild cognitive impairment, and also therapeutic in those with overt FTLD-tau, by decreasing

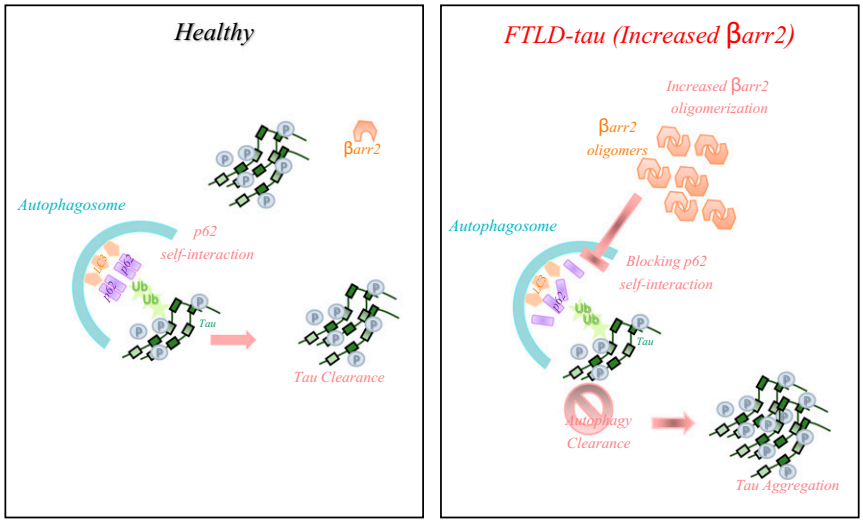

Fig. 7. Model of β-arrestin2-promoted tauopathy in FTLD. In healthy brains, monomeric β-arrestin2 regulates GPCR trafficking, and there is no excess of oligomeric β-arrestin2 and thus misfolded tau is efficiently ubiquitylated and targeted for autophagy clearance. However, in FTLD-tau brains, β-arrestin2 oligomers are increased, inhibiting p62-mediated autophagy, leading to failure of misfolded/aggregated tau to be efficiently cleared. In AD, the increased β-arrestin2 also results in an increase in Aβ amyloid (not illlustrated).

the existing tau tangles. Beyond tauopathy, it is conceivable that this strategy could also prove to be beneficial in other neurodegenerative diseases bearing proteinopathies that are cleared via p62.

Methods

Mice. *Arrb2*$^{-/-}$, tau P301S, and WT mice were all bred in the C57BL6 background for at least three generations prior to interbreeding with each other. The *Arrb2*$^{-/-}$ mice (66) and tau P301S mice (28) have previously been characterized. All experiments involving mice were performed in accordance with approved protocols by the Institutional Animal Care and Use Committee at the University of South Florida Health.

Patients Samples. Frozen frontal cortex tissue samples were obtained from the Alzheimer's Disease Research Center at Emory University. We used samples from FTLD-tau diagnosed patients (pathologically confirmed) and samples from nonaffected (control) patients who were otherwise matched as closely as possible for sex, age, and APOE genotype.

Primary Neuronal Cultures. Primary mouse hippocampal and cortical neuronal cultures were prepared from P0 mouse brains as previously described (29, 30, 67). Tissues were dissected in HBSS buffer and trypsinized with 0.25% trypsin-EDTA. The neurons were seeded on poly-D-lysine (Sigma-Aldrich) coated cover glasses or plates, and cultured in neurobasal media with B27 (Invitrogen) and glutamax (Invitrogen).

Antibodies and Reagents. The following antibodies were used for Western blotting and immunostaining in a manner previously reported (29): Tau A10 1:1,000 for Western blotting and 1:200 for immunostaining (Santa Cruz Biotechnology), pS199/202 1:1,000 for Western blotting and 1:200 for immunostaining (Invitrogen), PHF1 1:20 for Western blotting (a gift from Dr. Peter Davies, Albert Einstein College of Medicine, Bronx, NY), synaptophysin 1:200 for immunostaining (Invitrogen), drebrin 1:200 for immunostaining (Invitrogen), actin 1:5,000 for Western blotting (Sigma-Aldrich), Flag 1:1,000 for Western blotting and 1:200 for immunostaining (Sigma-Aldrich), HA 1:1,000 for Western blotting (Cell Signaling), Myc 1:1,000 for Western blotting and 1:200 for immunostaining (Cell Signaling), GFP 1:1,000 for Western blotting and 1:200 for immunostaining (Cell Signaling), and HT7 1:200 for immunostaining (Invitrogen).

DNA Constructs, siRNA, and shRNA Lentivirus. β-Arrestin2, β-arrestin2 ΔIP6C, and β-arrestin2 ΔIP6N constructs were kind a gift from S. Marullo, Institut Cochin, Paris, France. pCDNA-β-arrestin2-HA was from X. Xin, Shanghai Institute of Materia Medica, Shanghai, China. The following were obtained from Addgene: β-arrestin2 GFP WT plasmid 35411 (68), HA-p62 plasmid 28027 (69), pMXs-puro GFP-p62 plasmid 38277 (58), and pmRFP-LC3 plasmid 21075 (70). β-arrestin2 ON-TARGET plus SMART pool siRNA was purchased from Dharmacon. β-Arrestin2 shRNA construct was from Applied Biological Materials Inc. (ABM). HEK-293 cells were transfected with the Lenti-virus constructs, pVSVG, and Pax2 using polyethylenimine (PEI). After 72 h, viruses were obtained from the media using a syringe filter (0.2 to 0.45 μm) as previously described (29).

Proximity Ligation Assay. The assay was performed using commercially available reagents (29) (Duolink, Sigma-Aldrich) with transfection of HeLa-V5-tau cells with WT β-arrestin2-flag and β-arrestin2-myc, without and with the mutant β-arrestin2 ΔIP6C or β-arrestin2 ΔIP6N constructs. Cells were fixed with 4% paraformaldehyde for 15 min at 25 °C and washed with 0.2% Triton in TBS. After washing, cells were blocked in 3% goat serum with 0.2% Triton for 1 h at 25 °C. After incubating with primary antibodies overnight at 4 °C, cells were washed and incubated with the PLA probes at 37 °C for 1 h, washed with buffer A, and incubated with ligation solution at 37 °C for 30 min. After washing with buffer A, amplification solution was applied at 37 °C for 100 min. Cells were then washed and mounted for confocal imaging.

Immunocytochemistry and Immunohistochemistry. These studies were performed using methods similar to those we have previously published (29). Cells were fixed with 4% paraformaldehyde for 15 min at room temperature, washed with 0.2% Triton in TBS, and then blocked with 3% BSA with 0.1% Triton for 1 h. Cells were exposed to the primary antibodies at 4 °C for 12 h and the secondary antibodies for 45 min at 25 °C. Mice were perfused with PBS and fixed with 4% paraformaldehyde for immunohistochemical studies. The 25-μm sections were blocked with goat serum with 0.2% Triton for 1 h at 25 °C and then incubated with primary antibodies at 4 °C for 12 h, followed by secondary antibody incubation for 1 h at 25 °C. Confocal images were obtained with the Olympus FV10i confocal microscope. ImageJ software was used to quantitate the immunoreactive signals from the samples. Images were captured with the same intensity and exposure time. Investigators were blinded as to the conditions within an experiment duing image acquisition and quantification.

Brain Homogenates, Cell Lysis, and Protein Extraction. Brain homogenates and cultured cells were prepared as described (29). Unless otherwise indicated, they were lysed with RIPA buffer (50 mM Tris pH 7.4, 0.1% SDS, 2 mM ethlenediaminetetraacetic acid, 150 mM NaCl, 1% Nonidet P-40) with the inclusion of protease and phosphatase inhibitors, and the supernatants were used for Western blot analysis. Extraction with sarkosyl was carried out as previously described (29, 71). Briefly, brain homogenates were lysed with A68 buffer (10 mM Tris·HCl, pH 7.4, 0.8 M NaCl, 10% sucrose, 1 mM EGTA). The samples were then centrifuged at 400 × *g* for 20 min at 4 °C, and the supernatants were collected. Sodium lauroyl sarcosinate (final concentration 1%) was addeded to the supernatants and incubated for 1.5 h at room temperature. After the incubation, samples were centrifuged at 80,000 × *g*

for 30 min at room temperature, and the pellets were collected in 50 mM Tris·HCl, pH 7.4.

Quantitative RT-PCR. As previously described (29), quantitative RT-PCR was carried out for detection of tau and β-arrestin mRNA using the Roche Light-Cycler 96 System (Life Science). Total RNA was isolated from human brains or cell lines using TRIzol (Invitrogen). Reverse transcription was carried out with oligo(dT) primers and Moloney murine leukemia virus reverse transcriptase (Superscript III, Invitrogen), and the DNA was quantitated by real-time PCR using Syber green master mix (Invitrogen). The comparative threshold cycle (Ct) value was used to calculate the amplification factor, and the relative amounts of β-arrestin2 or tau were divided by values obtained with GAPDH primers. The primers were human β-arrestin2 forward: GGAAGCTGGGCCAG-CAT, human β-arrestin2 reverse: GGAAGCTGGGCCAGCAT; mouse β-arrestin2 forward: GGCAAGCGCGACTTTGTAG, mouse β-arrestin2 reverse: GTGAGGGT-CACGAACACTTTC; and mouse tau forward: GGCTCTACTGAGAACCTGAA, and mouse tau reverse: TCTGCTCCATGGTCTGTCTT.

Generation of rAAV9, Stereotaxic Procedures, and Electrophysiology. Recombinant rAAV9 viruses were generated by cotransfection of serotype vector expressing the gene of interest with pAAV9 and pXX6 in HEK-293 cells and subjected to purification as previously reported (29, 72). Mice anesthetized with isoflurane were injected using a 10-μL syringe with a 26-gauge needle at the following bilateral coordinates: anteroposterior 2.7 mm, lateral 2.7 mm, and vertical 3.0 mm. A total volume of 2 μL purified rAAV9 (1×10^{12} vg/mL) was injected per side using the convection-enhanced delivery method. Brain tissues were collected 2 mo after injections. Electrophysiological recordings were carried out in brain slices as we previously described (29, 67). Three-month-old WT, tau P301S, tauP301S/*Arrb2*$^{+/-}$, and tauP301S/*Arrb2*$^{-/-}$ slices (hippocampus) were dissected and subjected to LTP, PPF, and IO recordings for the indicated time periods.

Atomic Force Microscopy Imaging. Recombinant p62 (4 μg) with/without recombinant β-arrestin2 (0.2 μg) was prepared in aqueous solution. Samples were incubated for 2 h at 25 °C in 30 μL of aqueous solution. The 10 μL of solution was drop casted on freshly cleaved mica surfaces. After 20 min of adsorption, filtered distilled water was used to gently wash excessive solutions from the mica surface. The mica was left at room temperature until it was thoroughly dry followed by AFM imaging. Commercial PointProbe Plus Non-Contact/Tapping Mode - High Resonance Frequency - Au coating (Detector Side) cantilever (Nanosensors) with a nominal spring constant of 42 N/m and a resonant frequency of 330 kHz were used for AFM imaging.

Recombinant Proteins. His-tau BL21 was provided by L. Blair, University of South Florida Health Byrd Alzheimer's Institute, Tampa, FL. Tau WT (4R0N) was subcloned into pET28a vector and transformed into BL21-competent cells. His-β-arrestin2 was transformed into Rosetta-competent cells. Cells were resuspended in ice-cold lysis buffer (Tris 20 mM, pH 8.0, NaCl 150 mM, imidazole 10 mM) with protease inhibitors. pFast-p62-his construct was transformed into DH10Bac-competent cells. After blue-white screening, DH10Bac strains were chosen to express and amplify recombinant bacmids. Sf9 insect cells transfected with bacmid (midiprep from DH10Bac-competent cells) were cultured for 3 d with Sf900 II SFM medium, then P1 generation virus in medium was collected and added to new Sf9 cells. After 2 d of culture, Sf9 cells were harvested and lysed with lysis buffer (Tris 20 mM, pH 7.4, NaCl 150 mM, 1% Triton, 10 mM imidazole, with protease inhibitors). After sonicating the cells, the cells were centrifuged at 14,000 × *g* for 15 min and the supernatants incubated with Ni Sepharose. Recombinant proteins were eluted with ice-cold elution buffer (Tris 20 mM, NaCl 150 mM, 200 mM imidazole), after which proteins were dialyzed in dialysis buffer (Tris 20 mM, NaCl 150 mM, DTT 1 mM) overnight at 4 °C.

Statistical Analysis and Graphs. Statistical analyses were performed by Prism 6.0 software (GraphPad Software) using paired or unpaired Student's *t* tests, and one- or two-way ANOVA. ANOVA was followed by the indicated post hoc tests. Data are shown as representative experiments, graphs of mean ± SEM, or box plots showing each data point, the median, the interquartile range (IQR), and the maximal and minimal values.

Data Availability. All materials, data, and associated protocols are included in the text and in *SI Appendix*.

ACKNOWLEDGMENTS. We thank K. Nash (University of South Florida) for providing AAV9 constructs, L. Blair for providing Hela-V5-cells and His-tau BL21 strains, and S. Marullo and X. Xin for providing the β-arrestin2 constructs. We thank A. Levey and M. Gearing (Emory University) for providing patients samples (NIH P50 AG025688). This work was supported in part by grants from the NIH (R01AG059721-01A1 to J.-A.A.W. and 1R01AG053060-01A1 to D.E.K.).

1. D. J. Irwin *et al*., Frontotemporal lobar degeneration: Defining phenotypic diversity through personalized medicine. *Acta Neuropathol.* **129**, 469–491 (2015).
2. N. J. Cairns *et al*.; Consortium for Frontotemporal Lobar Degeneration, Neuropathologic diagnostic and nosologic criteria for frontotemporal lobar degeneration: Consensus of the Consortium for Frontotemporal Lobar Degeneration. *Acta Neuropathol.* **114**, 5–22 (2007).
3. K. A. Vossel *et al*., Tau reduction prevents Abeta-induced defects in axonal transport. *Science* **330**, 198 (2010).
4. M. Jin *et al*., Soluble amyloid beta-protein dimers isolated from Alzheimer cortex directly induce Tau hyperphosphorylation and neuritic degeneration. *Proc. Natl. Acad. Sci. U.S.A.* **108**, 5819–5824 (2011).
5. P. T. Nelson *et al*., Modeling the association between 43 different clinical and pathological variables and the severity of cognitive impairment in a large autopsy cohort of elderly persons. *Brain Pathol.* **20**, 66–79 (2010).
6. P. Tiraboschi, L. A. Hansen, L. J. Thal, J. Corey-Bloom, The importance of neuritic plaques and tangles to the development and evolution of AD. *Neurology* **62**, 1984–1989 (2004).
7. F. E. Matthews *et al*., Epidemiological pathology of dementia: Attributable-risks at death in the medical research council cognitive function and ageing study. *PLoS Med.* **6**, e1000180 (2009).
8. Y. Ni *et al*., Activation of beta2-adrenergic receptor stimulates gamma-secretase activity and accelerates amyloid plaque formation. *Nat. Med.* **12**, 1390–1396 (2006).
9. S. AbdAlla *et al*., Dominant negative AT2 receptor oligomers induce G-protein arrest and symptoms of neurodegeneration. *J. Biol. Chem.* **284**, 6566–6574 (2009).
10. A. Thathiah *et al*., The orphan G protein-coupled receptor 3 modulates amyloid-beta peptide generation in neurons. *Science* **323**, 946–951 (2009).
11. P. Bakshi, E. Margenthaler, V. Laporte, F. Crawford, M. Mullan, Novel role of CXCR2 in regulation of gamma-secretase activity. *ACS Chem. Biol.* **3**, 777–789 (2008).
12. B. Ray, P. K. Banerjee, N. H. Greig, D. K. Lahiri, Memantine treatment decreases levels of secreted Alzheimer's amyloid precursor protein (APP) and amyloid beta (A beta) peptide in the human neuroblastoma cells. *Neurosci. Lett.* **470**, 1–5 (2010).
13. G. M. Alley *et al*., Memantine lowers amyloid-beta peptide levels in neuronal cultures and in APP/PS1 transgenic mice. *J. Neurosci. Res.* **88**, 143–154 (2010).
14. R. Minkeviciene, P. Banerjee, H. Tanila, Memantine improves spatial learning in a transgenic mouse model of Alzheimer's disease. *J. Pharmacol. Exp. Ther.* **311**, 677–682 (2004).
15. H. Scholtzova *et al*., Memantine leads to behavioral improvement and amyloid reduction in Alzheimer's-disease-model transgenic mice shown as by micromagnetic resonance imaging. *J. Neurosci. Res.* **86**, 2784–2791 (2008).
16. U. Wilden, S. W. Hall, H. Kühn, Phosphodiesterase activation by photoexcited rhodopsin is quenched when rhodopsin is phosphorylated and binds the intrinsic 48-kDa protein of rod outer segments. *Proc. Natl. Acad. Sci. U.S.A.* **83**, 1174–1178 (1986).
17. C. A. Moore, S. K. Milano, J. L. Benovic, Regulation of receptor trafficking by GRKs and arrestins. *Annu. Rev. Physiol.* **69**, 451–482 (2007).
18. V. V. Gurevich, E. V. Gurevich, The structural basis of arrestin-mediated regulation of G-protein-coupled receptors. *Pharmacol. Ther.* **110**, 465–502 (2006).
19. T. Shinohara *et al*., Primary and secondary structure of bovine retinal S antigen (48-kDa protein). *Proc. Natl. Acad. Sci. U.S.A.* **84**, 6975–6979 (1987).
20. K. Yamaki, Y. Takahashi, S. Sakuragi, K. Matsubara, Molecular cloning of the S-antigen cDNA from bovine retina. *Biochem. Biophys. Res. Commun.* **142**, 904–910 (1987).
21. S. M. Hanson, D. J. Francis, S. A. Vishnivetskiy, C. S. Klug, V. V. Gurevich, Visual arrestin binding to microtubules involves a distinct conformational change. *J. Biol. Chem.* **281**, 9765–9772 (2006).
22. S. M. Hanson *et al*., Arrestin mobilizes signaling proteins to the cytoskeleton and redirects their activity. *J. Mol. Biol.* **368**, 375–387 (2007).
23. K. S. Nair *et al*., Direct binding of visual arrestin to microtubules determines the differential subcellular localization of its splice variants in rod photoreceptors. *J. Biol. Chem.* **279**, 41240–41248 (2004).
24. H. Gao *et al*., Identification of beta-arrestin2 as a G protein-coupled receptor-stimulated regulator of NF-kappaB pathways. *Mol. Cell* **14**, 303–317 (2004).
25. X. Song, E. V. Gurevich, V. V. Gurevich, Cone arrestin binding to JNK3 and Mdm2: Conformational preference and localization of interaction sites. *J. Neurochem.* **103**, 1053–1062 (2007).
26. N. Wu *et al*., Arrestin binding to calmodulin: A direct interaction between two ubiquitous signaling proteins. *J. Mol. Biol.* **364**, 955–963 (2006).
27. A. Thathiah *et al*., β-arrestin 2 regulates Aβ generation and γ-secretase activity in Alzheimer's disease. *Nat. Med.* **19**, 43–49 (2013).
28. Y. Yoshiyama *et al*., Synapse loss and microglial activation precede tangles in a P301S tauopathy mouse model. *Neuron* **53**, 337–351 (2007).
29. J. A. Woo *et al*., Activated cofilin exacerbates tau pathology by impairing tau-mediated microtubule dynamics. *Commun. Biol.* **2**, 112 (2019).
30. J. A. Woo *et al*., Enhanced tau pathology via RanBP9 and Hsp90/Hsc70 chaperone complexes. *Hum. Mol. Genet.* **26**, 3973–3988 (2017).

31. S. K. Milano, Y. M. Kim, F. P. Stefano, J. L. Benovic, C. Brenner, Nonvisual arrestin oligomerization and cellular localization are regulated by inositol hexakisphosphate binding. *J. Biol. Chem.* **281**, 9812–9823 (2006).
32. H. Storez *et al*., Homo- and hetero-oligomerization of beta-arrestins in living cells. *J. Biol. Chem.* **280**, 40210–40215 (2005).
33. A. Dinculescu *et al*., Insertional mutagenesis and immunochemical analysis of visual arrestin interaction with rhodopsin. *J. Biol. Chem.* **277**, 11703–11708 (2002).
34. M. Breitman *et al*., Silent scaffolds: Inhibition OF c-Jun N-terminal kinase 3 activity in cell by dominant-negative arrestin-3 mutant. *J. Biol. Chem.* **287**, 19653–19664 (2012).
35. V. V. Gurevich, J. L. Benovic, Visual arrestin interaction with rhodopsin. Sequential multisite binding ensures strict selectivity toward light-activated phosphorylated rhodopsin. *J. Biol. Chem.* **268**, 11628–11638 (1993).
36. V. V. Gurevich *et al*., Arrestin interactions with G protein-coupled receptors. Direct binding studies of wild type and mutant arrestins with rhodopsin, beta 2-adrenergic, and m2 muscarinic cholinergic receptors. *J. Biol. Chem.* **270**, 720–731 (1995).
37. S. M. Hanson *et al*., Each rhodopsin molecule binds its own arrestin. *Proc. Natl. Acad. Sci. U.S.A.* **104**, 3125–3128 (2007).
38. M. Kim *et al*., Conformation of receptor-bound visual arrestin. *Proc. Natl. Acad. Sci. U.S.A.* **109**, 18407–18412 (2012).
39. K. Palczewski *et al*., Characterization of a truncated form of arrestin isolated from bovine rod outer segments. *Protein Sci.* **3**, 314–324 (1994).
40. A. Pulvermüller, K. Schroder, T. Fischer, K. P. Hofmann, Interactions of metarhodopsin II. Arrestin peptides compete with arrestin and transducin. *J. Biol. Chem.* **275**, 37679–37685 (2000).
41. S. A. Vishnivetskiy *et al*., Few residues within an extensive binding interface drive receptor interaction and determine the specificity of arrestin proteins. *J. Biol. Chem.* **286**, 24288–24299 (2011).
42. T. Zhuang *et al*., Involvement of distinct arrestin-1 elements in binding to different functional forms of rhodopsin. *Proc. Natl. Acad. Sci. U.S.A.* **110**, 942–947 (2013).
43. C. Boularan *et al*., beta-arrestin 2 oligomerization controls the Mdm2-dependent inhibition of p53. *Proc. Natl. Acad. Sci. U.S.A.* **104**, 18061–18066 (2007).
44. I. Gaidarov, J. G. Krupnick, J. R. Falck, J. L. Benovic, J. H. Keen, Arrestin function in G protein-coupled receptor endocytosis requires phosphoinositide binding. *EMBO J.* **18**, 871–881 (1999).
45. P. J. Dolan, G. V. Johnson, A caspase cleaved form of tau is preferentially degraded through the autophagy pathway. *J. Biol. Chem.* **285**, 21978–21987 (2010).
46. E. S. Wong *et al*., Autophagy-mediated clearance of aggresomes is not a universal phenomenon. *Hum. Mol. Genet.* **17**, 2570–2582 (2008).
47. S. Kim *et al*., Fisetin stimulates autophagic degradation of phosphorylated tau via the activation of TFEB and Nrf2 transcription factors. *Sci. Rep.* **6**, 24933 (2016).
48. U. Krüger, Y. Wang, S. Kumar, E. M. Mandelkow, Autophagic degradation of tau in primary neurons and its enhancement by trehalose. *Neurobiol. Aging* **33**, 2291–2305 (2012).
49. Y. Wang, U. Krüger, E. Mandelkow, E. M. Mandelkow, Generation of tau aggregates and clearance by autophagy in an inducible cell model of tauopathy. *Neurodegener. Dis.* **7**, 103–107 (2010).
50. A. Caccamo, E. Ferreira, C. Branca, S. Oddo, p62 improves AD-like pathology by increasing autophagy. *Mol. Psychiatry* **22**, 865–873 (2017).
51. A. King *et al*., Mixed tau, TDP-43 and p62 pathology in FTLD associated with a C9ORF72 repeat expansion and p.Ala239Thr MAPT (tau) variant. *Acta Neuropathol.* **125**, 303–310 (2013).
52. E. Kuusisto, A. Salminen, I. Alafuzoff, Early accumulation of p62 in neurofibrillary tangles in Alzheimer's disease: Possible role in tangle formation. *Neuropathol. Appl. Neurobiol.* **28**, 228–237 (2002).
53. B. Terni *et al*., Mutant ubiquitin and p62 immunoreactivity in cases of combined multiple system atrophy and Alzheimer's disease. *Acta Neuropathol.* **113**, 403–416 (2007).
54. X. Zheng *et al*., Effect of p62 on tau hyperphosphorylation in a rat model of Alzheimer's disease. *Neural Regen. Res.* **7**, 1304–1311 (2012).
55. J. Ramesh Babu *et al*., Genetic inactivation of p62 leads to accumulation of hyperphosphorylated tau and neurodegeneration. *J. Neurochem.* **106**, 107–120 (2008).
56. Y. Xu, S. Zhang, H. Zheng, The cargo receptor SQSTM1 ameliorates neurofibrillary tangle pathology and spreading through selective targeting of pathological MAPT (microtubule associated protein tau). *Autophagy* **15**, 583–598 (2019).
57. B. Wurzer *et al*., Oligomerization of p62 allows for selection of ubiquitinated cargo and isolation membrane during selective autophagy. *eLife* **4**, e08941 (2015).
58. E. Itakura, N. Mizushima, p62 targeting to the autophagosome formation site requires self-oligomerization but not LC3 binding. *J. Cell Biol.* **192**, 17–27 (2011).
59. K. B. Larsen *et al*., A reporter cell system to monitor autophagy based on p62/SQSTM1. *Autophagy* **6**, 784–793 (2010).
60. S. Pankiv *et al*., p62/SQSTM1 binds directly to Atg8/LC3 to facilitate degradation of ubiquitinated protein aggregates by autophagy. *J. Biol. Chem.* **282**, 24131–24145 (2007).
61. G. Zaffagnini *et al*., p62 filaments capture and present ubiquitinated cargos for autophagy. *EMBO J.* **37**, e98308 (2018).
62. P. V. Arriagada, J. H. Growdon, E. T. Hedley-Whyte, B. T. Hyman, Neurofibrillary tangles but not senile plaques parallel duration and severity of Alzheimer's disease. *Neurology* **42**, 631–639 (1992).
63. B. J. Melancon, J. C. Tarr, J. D. Panarese, M. R. Wood, C. W. Lindsley, Allosteric modulation of the M1 muscarinic acetylcholine receptor: Improving cognition and a potential treatment for schizophrenia and Alzheimer's disease. *Drug Discov. Today* **18**, 1185–1199 (2013).
64. E. Angulo *et al*., A1 adenosine receptors accumulate in neurodegenerative structures in Alzheimer disease and mediate both amyloid precursor protein processing and tau phosphorylation and translocation. *Brain Pathol.* **13**, 440–451 (2003).
65. M. Mogi, M. Horiuchi, Effects of angiotensin II receptor blockers on dementia. *Hypertens. Res.* **32**, 738–740 (2009).
66. L. M. Bohn *et al*., Enhanced morphine analgesia in mice lacking beta-arrestin 2. *Science* **286**, 2495–2498 (1999).
67. J. A. Woo *et al*., Slingshot-Cofilin activation mediates mitochondrial and synaptic dysfunction via Aβ ligation to β1-integrin conformers. *Cell Death Differ.* **22**, 1069–1070 (2015).
68. S. K. Shenoy, R. J. Lefkowitz, Receptor-specific ubiquitination of beta-arrestin directs assembly and targeting of seven-transmembrane receptor signalosomes. *J. Biol. Chem.* **280**, 15315–15324 (2005).
69. W. Fan *et al*., Keap1 facilitates p62-mediated ubiquitin aggregate clearance via autophagy. *Autophagy* **6**, 614–621 (2010).
70. S. Kimura, T. Noda, T. Yoshimori, Dissection of the autophagosome maturation process by a novel reporter protein, tandem fluorescent-tagged LC3. *Autophagy* **3**, 452–460 (2007).
71. M. Hasegawa *et al*., TDP-43 is deposited in the Guam parkinsonism-dementia complex brains. *Brain* **130**, 1386–1394 (2007).
72. N. Carty *et al*., Convection-enhanced delivery and systemic mannitol increase gene product distribution of AAV vectors 5, 8, and 9 and increase gene product in the adult mouse brain. *J. Neurosci. Methods* **194**, 144–153 (2010).